

A GENERALIZED PLANE STRAIN FORMULATION FOR CONTINUOUS CASTING SIMULATION

José Risso , Alfredo Huespe and Alberto Cardona

CIMEC / CONICET-UNL, Guemes 3450,
3000 Santa Fe,
Argentina.

email: jrisso@intec.unl.edu.ar

Key Words: Solid mechanics, steel continuous casting, generalized plane strain.

Abstract. *Stress and plastic strain analysis are required to determine zones with risk of internal cracking in the early stages of solidification in steel continuous casting processes. The high computational cost of three-dimensional models with conveniently refined meshes puts a severe difficulty to use them in repetitive analysis required to determine cracking susceptibility associated with variations in metallurgical parameters.*

In this work, we describe numerical schemes based on the Generalized Plane Strain hypothesis, using bi-dimensional models with temporal advance along strand axis.

Solutions obtained with these models are compared with semi-analytical 1D ones,^{1,2} and with solutions of axisymmetrical Eulerian-Lagrangian models for billet continuous casting simulation.³ We find a good agreement with previous results, and a high reduction in computation time.

Finally, we apply GPS model in slab continuous casting simulation comparing thermal results with those obtained with three-dimensional models,³⁻⁵ describing stress and strain results, and remarking some important issues related to crack sensitivity analysis.

1 INTRODUCTION

Internal cracking of steel products obtained by continuous casting can easily occur in industrial applications. Its prevention entails one of the most important issues in the development of this technology. There is a vast literature analyzing different aspects of this problem. Whatever the cracking criteria may be, alternative prediction models use basically the mechanical stress-strain state at temperatures close to solidification as a fundamental input data set.

Weiner et al.¹ proposed the use of a simplified semi-analytical procedure to describe, approximately, the evolution of stresses in this zone. Kristiansson² presented a finite element numerical scheme using the same fundamental hypothesis, the generalized plane strain condition (GPS). From there, the GPS assumption has been widely used in the literature for thermal stress evaluation in continuous casting simulations. However, models based on this hypothesis can not reproduce, a priori, tensional state near corners, which is a critical zone in slab continuous casting.

We propose a Generalized Plane Strain (GPS) finite element model in section 2.1. First, it is validated with the above mentioned studies. Then, we compare its results in a billet continuous casting simulation with an alternative eulerian-lagrangian procedure where no GPS condition is assumed (see Fachinotti³). This allows us to get an estimation of the GPS model validity for additional studies. Finally, in section 5 and using the GPS model, we present detailed results of a slab continuous casting simulation.

2 DESCRIPTION OF THE MECHANICAL PROBLEM

In a first approach for thermal analysis in the solid shell, a stationarity condition could be assumed, with an average casting velocity \mathbf{v}_c for the strand. The stress analysis proceeds by assuming an elastoplastic or viscoplastic material behavior with parameters strongly dependent on temperature.

Let us initially assume a Lagrangian description for the mechanical simulation of this process (see figure:1). We consider for every body point, and its neighborhood, three different configurations: i) the reference configuration, where the point label is assigned; ii) the (intermediate) natural configuration corresponding to the coordinates where the point has solidified; and iii) the actual point configuration. By denoting \mathbf{u}^o the point displacement from the reference to the natural configuration, \mathbf{u}^t the displacement from the reference to the actual configuration and \mathbf{u} the displacement from the natural to the actual configuration, it results:

$$\mathbf{u}^t = \mathbf{u}^o + \mathbf{u} \quad (1)$$

When a finite element procedure is used, normally the mesh is defined in the reference configuration, as depicted schematically in figure:1-b. In this picture we represent the reference domain (B) as the set of points at the top of the mould at time $t = 0$.

Let us consider that \mathbf{X} and \mathbf{x}^o are coordinate systems in the reference and natural configurations. The assumption of small deformation we introduce to describe the motion

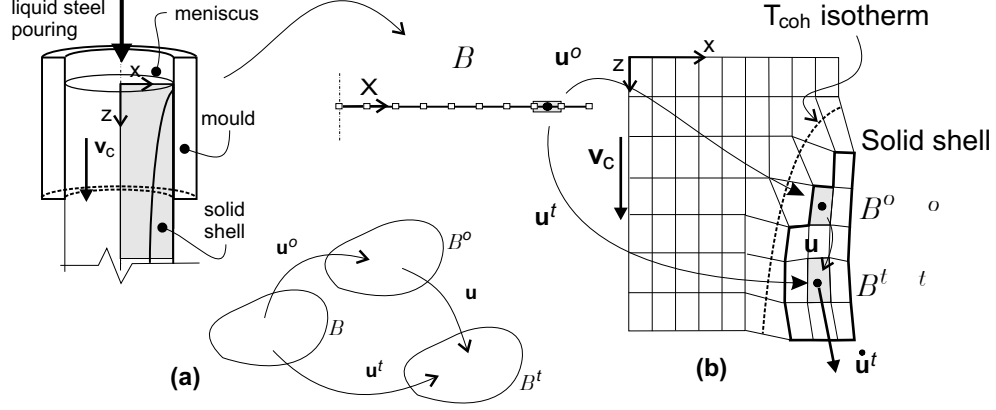


Figure 1: Reference (B), natural (B^o) and actual (B^t) body configurations

allows us to evaluate the strain $\varepsilon = \nabla_{\mathbf{x}^o}^{sym} \mathbf{u}$, related to the motion from natural to final configurations, by the following approaching term :

$$\varepsilon = \nabla_{\mathbf{x}^o}^{sym} \mathbf{u} \approx \nabla_{\mathbf{X}}^{sym} \mathbf{u} \quad (2)$$

and therefore, to admit the strain addition validity :

$$\varepsilon^t = \varepsilon + \varepsilon^o \quad (3)$$

where: $\varepsilon^t = \nabla_{\mathbf{X}}^{sym} \mathbf{u}^t$ is the strain at the actual configuration (at time t) with respect to the reference configuration, and $\varepsilon^o = \nabla_{\mathbf{X}}^{sym} \mathbf{u}^o$ the strain in natural configuration with respect to the reference one.

Mechanical strains ε_M , are computed from ε by subtracting the thermal strain ε_θ :

$$\varepsilon_M = \varepsilon - \varepsilon_\theta \quad ; \quad \varepsilon_\theta = \beta(\theta) \mathbf{1} \quad (4)$$

with $\beta(\theta)$ as the thermal expansion. Stresses in the solid shell are a function of them.

Adopting the classical J_2 elastoplastic theory with isotropic hardening, the stress-strain relation results from:

$$\sigma = \mathbf{C}^e(\theta) \cdot (\varepsilon_M - \varepsilon_M^p); \quad (5)$$

$$\dot{q} = -H(\theta) \dot{\kappa} \quad (6)$$

$$\dot{\varepsilon}_M^p = \lambda \mathbf{n} \quad ; \quad \mathbf{n} = \frac{\sigma_{dev}}{\|\sigma_{dev}\|} \quad (7)$$

$$\dot{\kappa} = \lambda \sqrt{\frac{2}{3}} \quad (8)$$

$$\lambda \geq 0 \quad ; \quad \phi(\sigma, q, \theta) \leq 0 \quad ; \quad \phi\lambda = 0 \quad (9)$$

$$\phi(\sigma, q, \theta) = \sqrt{\sigma_{dev} \cdot \sigma_{dev}} - \sqrt{\frac{2}{3}}(\sigma_y(\theta) - q) \quad (10)$$

where $\mathbf{C}^e(\theta)$ is the elastic constitutive tensor

$$\mathbf{C}^e = \hat{\lambda}(\theta)(\mathbf{1} \otimes \mathbf{1}) + 2\mu(\theta)\mathbf{I},$$

with $(\hat{\lambda}, \mu)$ the Lamé's parameters, ε_M^p the plastic strain, and $\mathbf{1}$, \mathbf{I} the 2nd and 4th order identity tensors. The scalar internal variables q , like a stress, describes the isotropic strain hardening that is related to its conjugate internal variable, κ , through the plastic modulus H (see equation (6)). Equations (7) and (8) are the classical associative flow laws defining the evolution of the strain-type internal variables. Typically, the deviatoric stress σ_{dev} in equation (7) defines the direction of the plastic strain rate.

Finally, expressions (9) are the consistency relations, being $\phi(\sigma, q, \theta)$ the yield criteria (Von Mises in our case, eq.(10), where $\sigma_y(\theta)$ is the yield stress) and λ the plastic multiplier.

2.1 Generalized plane strain model: pure lagrangian description

The instantaneous velocity of a point in the solid shell $\dot{\mathbf{u}}^t$ can be seen as resulting from the addition of two terms: the average casting velocity \mathbf{v}_c in the direction of z axis (see figure 1), and a relative velocity $\dot{\mathbf{u}}^r$ defined with respect to an observer moving with velocity \mathbf{v}_c :

$$\dot{\mathbf{u}}^t = \mathbf{v}_c + \dot{\mathbf{u}}^r \quad ; \quad \dot{\mathbf{u}}^r = (\dot{u}_x^r, \dot{u}_y^r, \dot{u}_z^r) \quad (11)$$

The generalized plane strain condition (GPS) assumes that $\dot{\varepsilon}_z = \frac{\partial \dot{u}_z^r}{\partial z}$ is uniform in (x, y) (see figure 2), that is, this strain component does not depend on coordinates (x, y) . Furthermore, it is assumed that $\dot{\varepsilon}_{xz} \approx \dot{\varepsilon}_{yz} \approx 0$. Both conditions require the independence of u_x^r and u_y^r with coordinate z . In some regions of the solid, this assumption is clearly not convincing.

The term $\dot{\varepsilon}_z$ can be implicitly treated in the analysis by considering the equilibrium equation in z direction. The free traction boundary condition at the upper and bottom part of the slab imposes, in all z -constant sections, that:

$$\int_A \sigma_z(x, y) dx dy = 0. \quad (12)$$

This equation makes it possible to project the 3-D model to a plane problem and its posterior numerical treatment as if it were a pure 2-D mechanical state. We observe that the equations of this model result from the transformation of the stationary advection hyperbolic problem to a parabolic one where the time should be introduced as a primal variable.

2.1.1 Implementation of a generalized plane strain FE model

We implement the generalized plane strain condition for the modelling of a slab continuous casting process, by adopting a reference domain lying on the plane (x, y) , see figure 2. The domain is discretized using standard bilinear quadrilateral four node elements, which include an additional degree-of-freedom that accounts for the deformation component ε_z . The strain-displacement matrix \mathbf{B} is taken as:

$$\mathbf{B}^{4 \times 9} = \begin{pmatrix} \mathbf{B}_1^{qst} & \mathbf{B}_2^{qst} & \mathbf{B}_3^{qst} & \mathbf{B}_4^{qst} & \mathbf{0} \\ \mathbf{0} & \mathbf{0} & \mathbf{0} & \mathbf{0} & 1 \end{pmatrix} \quad (13)$$

where \mathbf{B}_i^{qst} is the i^{th} block of the standard strain-displacement matrix of the bilinear quadrilateral element:

$$\mathbf{B}_i^{qst} = \begin{pmatrix} \frac{\partial N_i}{\partial x} & 0 \\ 0 & \frac{\partial N_i}{\partial y} \\ \frac{\partial N_i}{\partial y} & \frac{\partial N_i}{\partial x} \end{pmatrix}$$

and $N_i(x, y)$ the corresponding shape function of node i . The generalized displacement elemental vector results :

$$\hat{\mathbf{a}}^T = [u_1^x \ u_1^y \ \dots \ u_4^x \ u_4^y \ \hat{\varepsilon}^z] \quad (14)$$

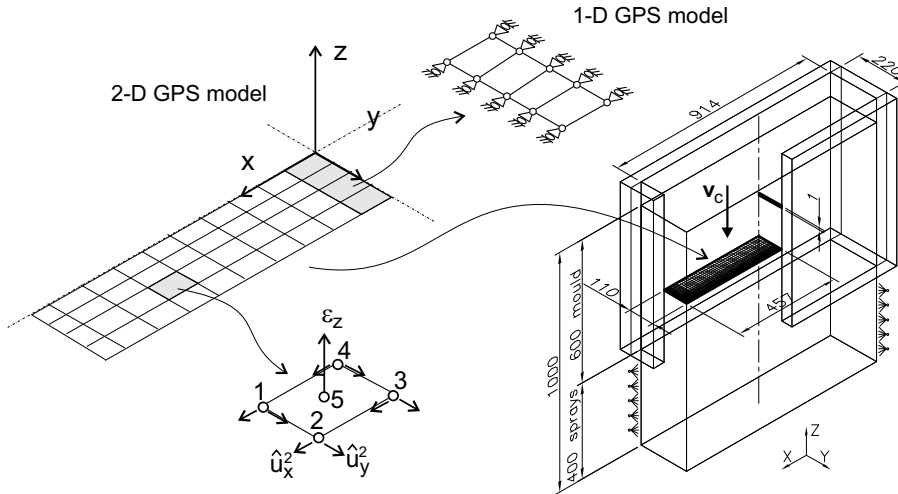


Figure 2: Generalized plane strain model of a slab continuous casting process.

The additional degree-of-freedom $\hat{\varepsilon}^z$ is shared by all elements in the mesh. It is numbered as the last global discrete system d.o.f.. In this way, the coupling introduced by the equilibrium equation (12) does not substantially change the skyline of the structural stiffness matrix, and therefore, the computational cost is similar to a 2-D analysis.

The strain ε^o is stored at the finite element Gauss points as an additional tensorial internal variable in the first time step where all nodal temperatures of the element fall below the zero strength temperature (ZST).

Changes in the solid shell domain introduce difficulties concerning the mesh definition. The implemented procedure defines a mesh that describes the complete domain, including liquid and mushy zones. Nodes in the mushy zone are initially fixed and without stiffness. In subsequent time steps, when the nodal temperature falls below the ZST, they are freed.

The above described numerical model does not predict a correct displacement field inside the solid shell. However, displacements of the shell surface points are well approximated, which is important for a correct prediction of the strand-mould air gap formation. In the surface of a billet, for instance, differences between displacements calculated with GPS and eulerian-lagrangian models are lower than 5%.

2.2 Mechanical model based on an eulerian-lagrangian description

An alternative model is used to compare GPS results in billet continuous casting simulation, where symmetry of revolution in the thermal and mechanical problem is assumed. This model removes the hypothesis of $\dot{\varepsilon}_z$ uniformity in z-constant planes, typical from the GPS one. The reference configuration is a 2-D domain as shown in figure:3 that only represent the solid shell. The x-coordinate represents the billet radial direction.

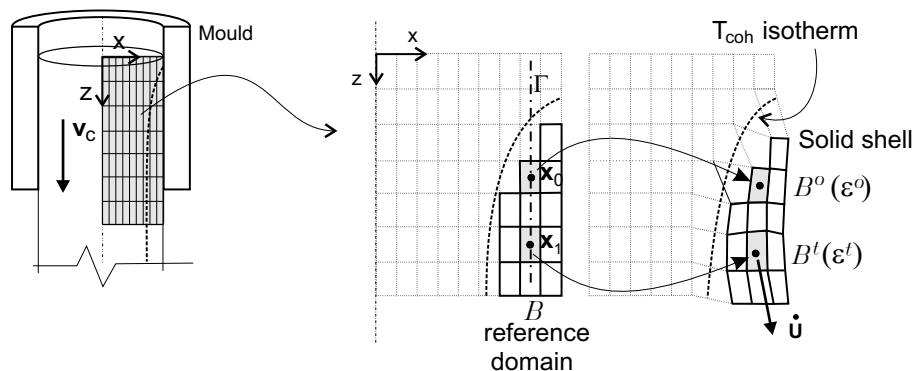


Figure 3: Eulerian-lagrangian model for simulating the billet continuous casting.

From the numerical point of view, this model is easily implemented in a standard elastoplastic finite element code using structured meshes. It is necessary, for every element in the mesh, to include a pointer to a preceding element belonging to the same streamline Γ , to construct a relationship between a Gauss point and its homologue in the previous element. The constitutive model equations uses this relation to obtain the historical variables at the previous time.

The discrete equilibrium equations are solved using a standard Newton method. The Jacobian matrix corresponds to that obtained from an equivalent elastoplastic quasi-static

incremental problem, and is not consistent with the numerical integration scheme, but we have obtained converged solutions using rather adjusted tolerances without an excessive number of Newton iterations. A detailed formulation of this model, including a consistent matrix and its numerical performance, was presented in Fachinotti.³

3 VALIDATION OF THE NUMERICAL MODEL

Let us consider the early stage of a slab continuous casting process such as that shown in fig.2, and particularly the region corresponding to the wide side central part of the solid shell. Thermal stresses can be evaluated by assuming generalized plane strain condition in z and x directions because there exists free traction condition on all vertical slab sides. Of course, this hypothesis neglects any shell curvature effect on stresses.

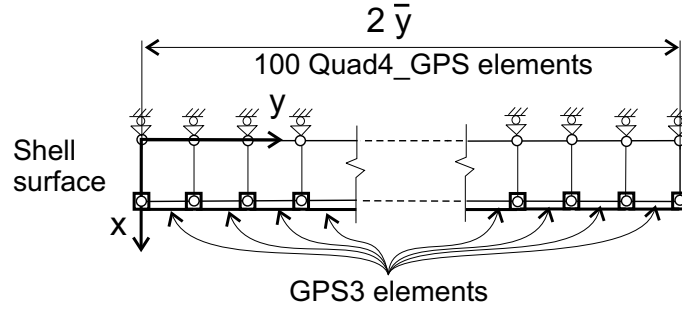


Figure 4: Finite element model for the 1-D numerical validation test (see figure 2)

Following this particular assumption, Weiner et al.¹ determined a simplified 1-D semi-analytical solution. The thermal problem corresponds to the Neumann's classical one, a phase change with uniform initial temperature T^s (solidus) and fixing a temperature T^o on one end (shell surface in fig.2). For the mechanical problem, they took an elastic-perfectly plastic material model, with a constant Young modulus E and yield stress σ_y varying linearly with temperature:

$$\sigma_y(T) = \sigma_y^o \frac{T^s - T}{T^o} \quad ; \quad T \leq T^s \quad (15)$$

where σ_y^o is the yield stress at temperature T^o .

Neumann's solution introduces a characteristic length $\bar{y} = p\sqrt{(t)}$, where t is the time and p the parameter given by:

$$p = 2K_s\gamma \quad ; \quad K_s = \frac{\kappa}{\rho C_p} \quad ; \quad \gamma \approx \sqrt{\frac{T^o C_p}{2L}} \quad (\gamma^2 \ll 1); \quad (16)$$

where the thermal diffusivity K_s is the ratio of conductivity (κ) with density (ρ) and with specific heat (C_p), while L is the latent heat.

Weiner et al. also introduced the dimensionless quantities:

$$\hat{y} = \frac{y}{\bar{y}} \quad ; \quad \hat{T} = \frac{T - T^s}{T^o}$$

$$\hat{\sigma} = \frac{(1 - \nu)\sigma}{\alpha ET^o} \quad ; \quad \hat{\sigma}_y = \frac{(1 - \nu)\sigma_y}{\alpha ET^o} = -m\hat{T} \quad ; \quad m = \frac{(1 - \nu)\sigma_y^o}{\alpha ET^o}$$

where α is the thermal expansion coefficient and ν the Poisson's ratio.

We have solved this problem assuming GPS condition in directions z and x . The FE mesh, as shown in figure: 4, consists of 100 Quad4_GPS elements. The GPS condition in the x -direction ($\varepsilon_x = \text{constant}$) is imposed via Lagrange multipliers.

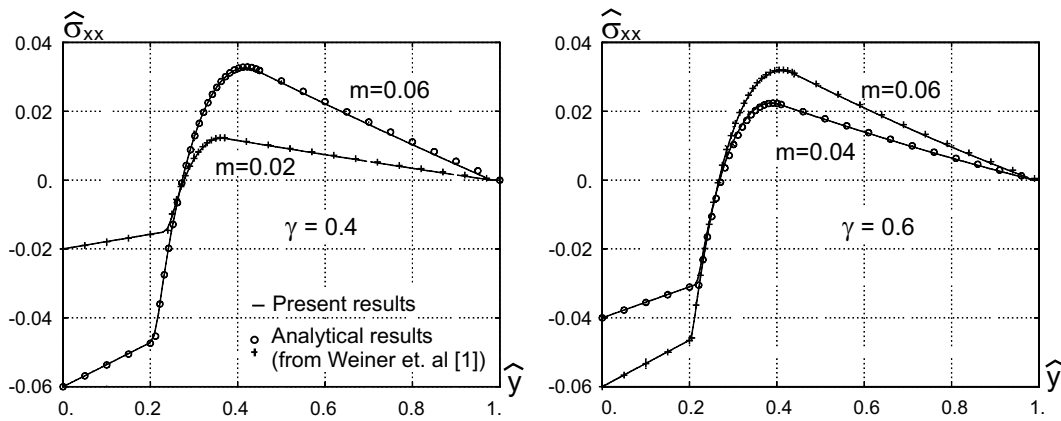


Figure 5: Analytical vs. numerical stress distribution along the \hat{y} -coordinate, 1-D problem.¹

Figures 5 compare the semi-analytical results and the numerical ones. The curves plot the non-dimensional stress component $\hat{\sigma}_{xx}(= \hat{\sigma}_{zz})$ along the non-dimensional \hat{y} -line (surface shell depth) for different values of m and γ parameters. The agreement of the numerical FE solutions with the semi-analytical ones is evident from the figure.

This solution gives a constant maximum tensile (compressive) stress along the time. This behavior is due to the particular thermal boundary conditions adopted (similarity solution) in the study. However, they show a stress distribution trend similar to that observed in more complex solidification problems.

4 BILLET CONTINUOUS CASTING ANALYSIS

In this section we analyze the early stage of a billet continuous casting process, including the mould exit zone. We compare FE results obtained either by imposing the GPS condition or by using the eulerian-lagrangian axisymmetric model of section 2.2.

Tests were made using 0.3%C carbon steel. Material parameters and problem data are specified in Table 1 (taken from Perez et al.⁶):

Parameter	Symb.	Value	Parameter	Symb.	Value
Density	ρ	7200[kg/m ³]	Solidus temp.	T_s	1490[°C]
Specific Heat	C_p	680[J/kg°C]	Liquidus temp.	T_l	1501[°C]
Latent Heat	L	272000[J/kg]	Zero Strength temp.	ZST	1495[°C]
Conductivity (solid)	κ_s	34[W/m°C]	Pouring temp.	T_p	1530[°C]
Conductivity (liq.)	κ_l	68[W/m°C]			

Table 1: Material and problem data for the analyzed billet continuous casting process

Following Kelly et al.,⁷ the liquid conductivity κ_l is larger than the solid conductivity κ_s because of turbulence in the liquid pool. The casting speed v_c was assumed to be 1.6 [m/s], and the thermal boundary conditions are:

- a) prescribed flux in the mould–slab interface (using Savage-Pritchard law^{8,9}):

$$\mathbf{q}[MW/m^2] = - \left(3.071 - 0.361 \sqrt{\frac{\Delta z}{v_c}} \right), \quad (17)$$

where $\Delta z[m]$ is the z-distance from the meniscus;

- b) convective flux, due to sprays,¹⁰ below the mould exit (using a convection coefficient $h_s = 0.5[MW/(m^2 \cdot °C)]$ and $T_{spray} = 40[°C]$).

$$\mathbf{q}[MW/m^2] = h_s(T_{surface} - T_{spray}), \quad (18)$$

A J_2 plasticity model with isotropic hardening¹¹ is used. Figure 6-a is a schematic diagram of the problem geometry while Figure 6-b displays the material parameters as function of temperature.

4.1 Comparison between the GPS and eulerian-lagrangian models

The GPS scheme is solved using a mesh of 75 Quad4 axisymmetric elements (fig.6), and GPS condition is imposed via Lagrange multipliers (GPS3 elements). The incremental time step is defined to match the axial discretization of the eulerian-lagrangian scheme. The eulerian-lagrangian model uses a 2D mesh with the 75 elements in the radial direction, and 100 elements in the axial direction.

Comparing axial (or circumferential) stresses, see figure 7-a, we find a good agreement between both results, except in sections near the mould exit. There, it is expected an incorrect stress prediction of the GPS model because of the sudden change of thermal boundary conditions. The same behavior is found for radial stresses (even considering that radial stresses are one order of magnitude lower than axial or circumferential stresses). Figure 7-b shows a noticeable difference in the peak stress predicted in the mould exit zone, but it happens in a very thin superficial region.

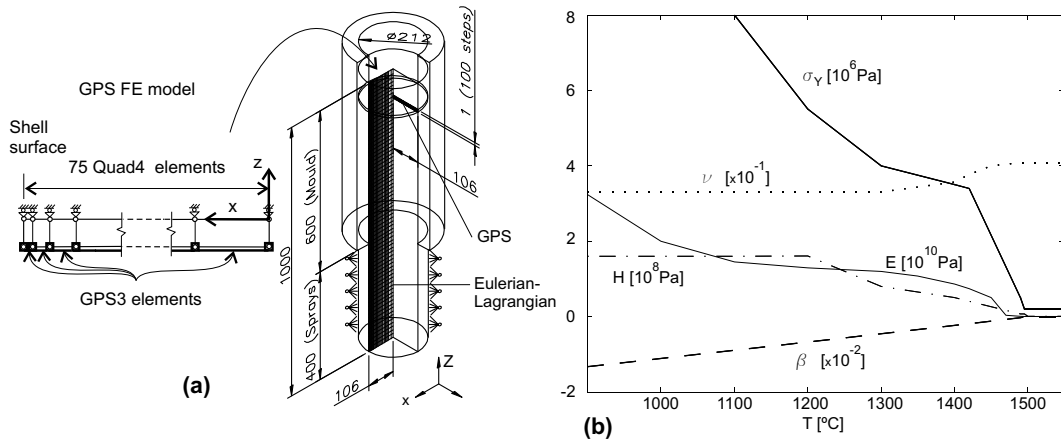


Figure 6: Billet continuous casting simulation. **a)**: geometry and GPS model. **b)**: Temperature-dependent parameters; E : Young's modulus, ν : Poisson's ratio, H : Hardening modulus, σ_Y : yield stress and β : thermal expansion function.

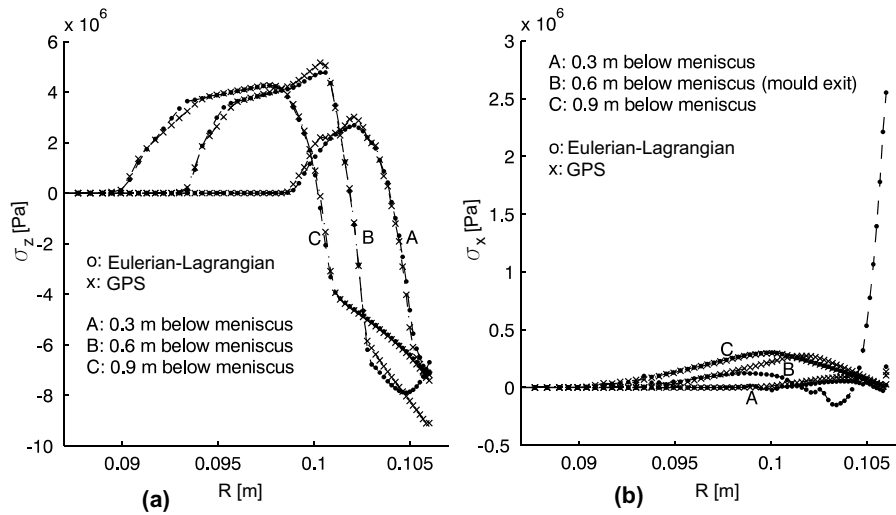


Figure 7: Billet continuous casting simulation. Comparison of computed: **a)** axial and **b)** radial stresses

Figure 8 shows a good agreement for the plastic strains prediction. This observation have important consequences when the crack criterion is based on the total applied strain (see Yamanaka et al.¹²).

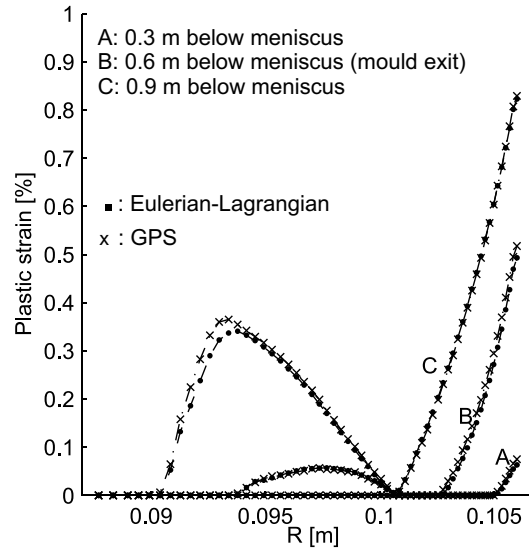


Figure 8: Billet continuous casting simulation. Comparison of computed plastic strains

5 APPLICATION TO A SLAB CONTINUOUS CASTING PROCESS

Figure 9 displays the schematic diagram and geometrical data of the simulated problem. Casting material is low carbon steel.¹³

Parameter	Symb.	Value	Parameter	Symb.	Value
Density	ρ	7200[kg/m ³]	Solidus temp.	T_s	1518[°C]
Specific Heat	C_p	680[J/kg°C]	Liquidus temp.	T_l	1532[°C]
Latent Heat	L	272000[J/kg]	Zero Strength temp.	ZST	1518[°C]
Conductivity (solid)	κ_s	34[W/m°C]	Pouring temp.	T_p	1562[°C]
Conductivity (liq.)	κ_l	68[W/m°C]			

Table 2: Material and problem data of the slab continuous casting simulation.

Casting speed is 1.0 [m/s] and thermal boundary conditions are:

- a) prescribed flux in the mould–slab interface (using Savage-Pritchard law^{8,13})

$$\mathbf{q}[MW/m^2] = -(2.68 - 2.58\sqrt{\Delta z}), \quad (19)$$

Remark: following Thomas et al.,¹³ in a band of 31 mm wide from the slab corner, we decrease this flux value by 0.67, because of the gap increment in this zone.

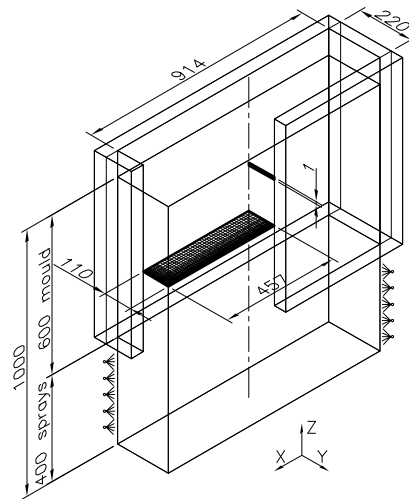


Figure 9: Slab continuous casting process. Schematic diagram.

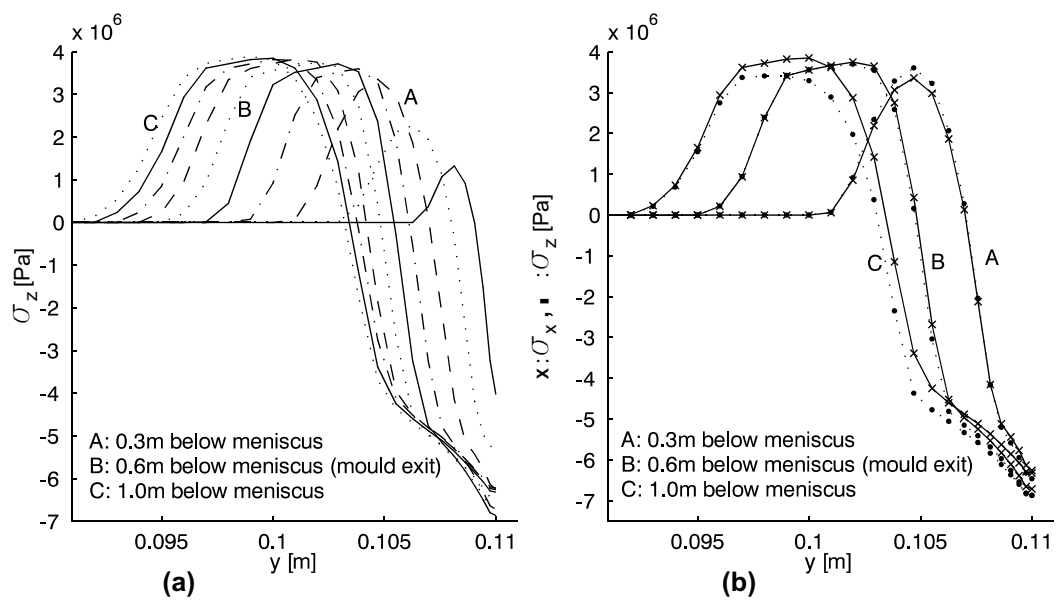


Figure 10: Slab continuous casting problem: a) evolution of σ_x stress component in the wide face mid-section (every 0.1[m]); b) comparison of σ_x and σ_z stress components in the wide face mid-section.

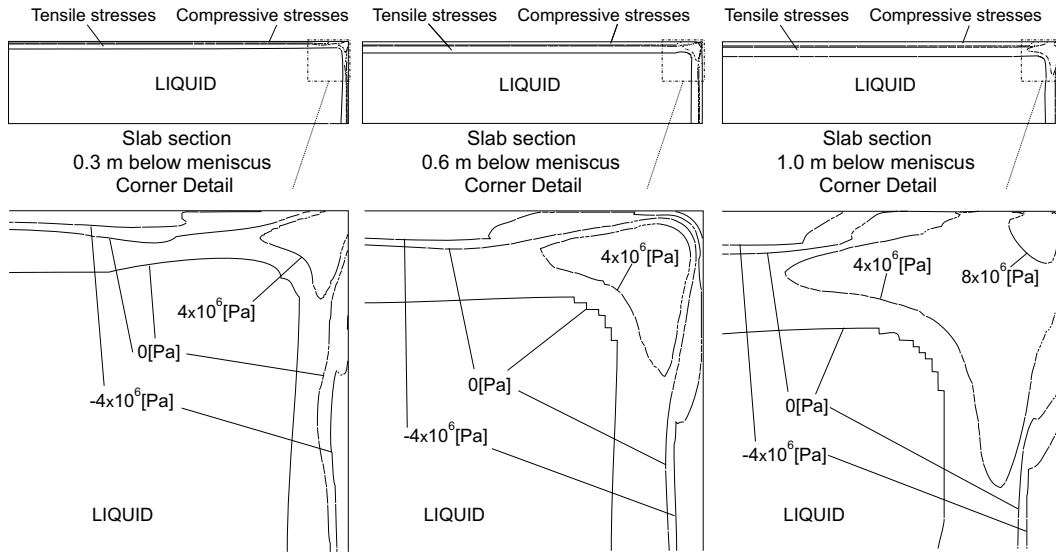


Figure 11: Slab continuous casting problem. Evolution of σ_z stresses during solidification.

- b)** convective flux due to sprays¹⁰ (using $h_s = 0.5[MW/(m^2 \cdot ^\circ C)]$ and $T_s = 40[^\circ C]$).

$$\mathbf{q}[MW/m^2] = h_s(T_{surface} - T_{spray}), \quad (20)$$

As shown in figure 10-a, the stress evolution component σ_x in the upper zone of the mould, where the slab surface temperature drops significantly, is very different from that predicted by Weiner's model. The difference is less important in zones where surface temperatures are more uniform. Calculated values of σ_x and σ_z in the wide face mid-section are very similar, as can be seen in Figure 10-b.

Figure 11 show a detail of the axial stress distribution (σ_z) in three different sections of the slab corner along the strand. We note that tensile stresses appear in the shell surface, even though in the remaining part of the slab surface we observe compressive stresses.

The analysis of plastic strains in fig.13 and fig.12 shows values which are two times larger in the corner zones than in the face mid-section ones. Moreover, we see plastic strain peaks appearing in two bands, parallel to corner's edge. Experimental evidence shows that this zone is prone to imperfections.

6 CONCLUSIONS

We conclude:

- a)** The semi-analytical solution of Weiner et al. describe a correct tendency for stress distribution, at least in the billet and center of wide side slab cases; however the peak stresses, a fundamental result for crack analysis, are not correctly predicted.

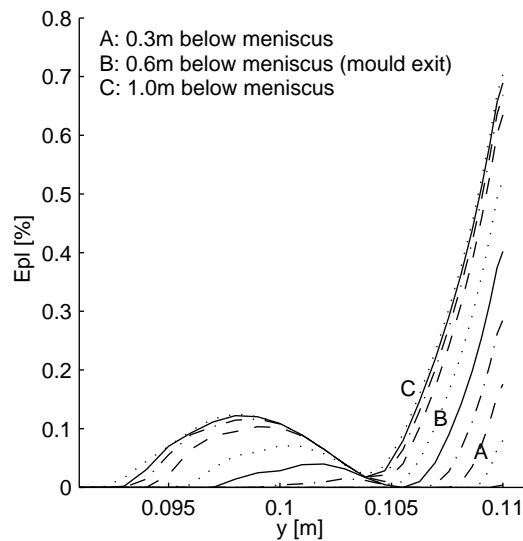


Figure 12: Slab continuous casting problem. Evolution of the wide face mid-section plastic strains.

b) The solution obtained with our GPS model agrees well with results of the eulerian-lagrangian model in billet continuous casting simulation. Thermal results match very well, and mechanical results show good agreement except in a small zone close to the mould exit.

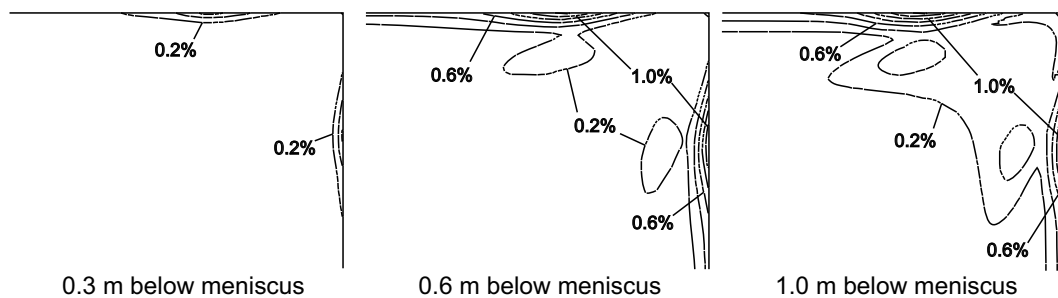


Figure 13: Slab continuous casting problem. Evolution of plastic strains close to the slab corner.

The agreement degree between the mechanical GPS model results and the eulerian-lagrangian ones gives a good basis to apply the first procedure in the slab continuous casting process simulation.

A remarkable characteristic of the GPS model is its low computational cost. This makes the GPS model suitable for future research works involving determination of parameters for cracking susceptibility.

REFERENCES

- [1] Weiner J.H. and Boley B.A. Elasto-plastic thermal stresses in a solidifying body. *J. Mech. Phys. Solids*, **11** (1963).
- [2] Kristiansson J.O. Thermal stresses in the early stage of solidification of steel. *J. of Thermal Stresses*, **5** (1982).
- [3] Fachinotti V.D. Modelado numérico de fenómenos termomecánicos en la solidificación y enfriamiento de aceros obtenidos por colada continua. *Tesis Doctoral, Universidad Nac. Litoral, Argentina*, (2001).
- [4] Fachinotti V.D., Cardona A., and Huespe A. A fast, convergent and accurate temperature model for phase-change heat conduction. *Int.J.Num.Meth.Eng.*, **44** (1999).
- [5] Huespe A.E., Cardona A., and Fachinotti V.D. Thermomechanical model of a continuous casting process. *Comp. Meth. Appl. Mech. Eng.*, **182** (2000).
- [6] Perez T., Goldschmit M., Dvorkin E., Nigro N., Storti M., and Idelsohn S. Segregación dendrítica de aceros obtenidos por colada continua. iii. resolución numérica de la macrosegregación en un acero 1040 fabricado por siderca. *Reporte Técnico CINI-FUDETEC GTM-INTEC Septiembre 1997*, (1997).
- [7] Kelly J.E., Michalek K.P., O'Connor T.G., Thomas B.G., and Dantzig J.A. Initial development of thermal and stress fields in continuously cast steel billets. *Metall. Trans. A*, **19A** (1982).
- [8] E.T.Linacre and J.C. Crane. Heat transfer rate in a water-cooled mould. *In J. Savage and W.H. Pritchard: The problem of the rupture of the billet in the continuous casting of steel. J. Iron and Steel Inst.*, **178** (1952).
- [9] Dvorkin E. and Canga M. Thermomechanical behavior of the mold in siderca continuous casting machine cc3. case of ϕ 295 mm and carbon steel 042. *Reporte Técnico I 1.20/190-90, CINI*, (1990).
- [10] El-Bealy M. On the mechanism of halfway cracks and macro segregation in continuously cast steel slabs.(i) halfway cracks. *Scandinavian J. Metall.*, **24** (1995).
- [11] Fachinotti V.D. and Cardona A. Constitutive models of steel under continuous casting conditions. *J. Materials Processing Technology*, **135** (2003).
- [12] Yamanaka A., Nakajima K., and Okamura K. Critical strain for internal crack formation in continuous casting. *Ironmaking and Steelmaking*, **22**(6) (1995).
- [13] Thomas B.G., Li G., Moitra A., and Habing D. Analysis of thermal and mechanical behavior of copper molds during continuous casting of steel slabs. *ISS Trans.*, (1998).